Title

3D Deformation Behavior of Geosynthetic-Reinforced Soil Bridge Abutments

Authors

Rong, Wenyong
Zheng, Yewei
McCartney, John S
et al.

Publication Date

2017-03-30

DOI

10.1061/9780784480458.005

Peer reviewed

3D Deformation Behavior of Geosynthetic-Reinforced Soil Bridge Abutments

Wenyong Rong[1], M.S., S.M. ASCE, Yewei Zheng[2], M.S., S.M. ASCE, John S. McCartney[3], Ph.D., P.E., M. ASCE, Patrick J. Fox[4], Ph.D., P.E., F. ASCE

[1]Graduate Research Assistant, Department of Structural Engineering, University of California, San Diego, La Jolla, CA 92093-0085; Email: w1rong@eng.ucsd.edu
[2]Graduate Research Assistant, Department of Structural Engineering, University of California, San Diego, La Jolla, CA 92093-0085; Email: y7zheng@ucsd.edu
[3]Associate Professor, Department of Structural Engineering, University of California, San Diego, La Jolla, CA 92093-0085; Email: mccartney@ucsd.edu
[4]Shaw Professor and Head, Department of Civil and Environmental Engineering, Pennsylvania State University, University Park, PA 16802; Email: pjfox@engr.psu.edu

ABSTRACT

Although 2-dimensional (2D) design methods have been shown to work well in defining the longitudinal reinforcement layout in geosynthetic-reinforced soil (GRS) bridge abutments, three-dimensional (3D) effects may play a role in the design of the side walls and the associated transverse reinforcement layout. The objective of this study is to understand the deformation behavior of GRS bridge abutments considering 3D boundary effects, using finite difference analyses to simulate the deformation behavior of a hypothetical GRS bridge abutment expected during construction. Soil-concrete and concrete-concrete interactions were simulated using interface elements and soil-geogrid interactions were simulated using geogrid structural elements. Analyses were performed in stages to simulate the abutment construction process with different reinforcement vertical spacing and length. The results presented in this paper provide insight into the lower wall lateral facing displacements in both the longitudinal and the transverse directions, as well as bridge seat settlements at different sections. This information is a useful component in the development of comprehensive design guidance for GRS bridge abutments.

INTRODUCTION

Geosynthetic-reinforced soil (GRS) bridge abutments have many advantages over conventional pile-supported bridge abutment designs, including lower cost, faster construction, as well as good performance under static and seismic loads (Helwany et al. 2003). In most instances, GRS bridge abutments are a system that includes a lower GRS supporting a bridge seat (i.e., a shallow footing) upon which the bridge deck rests and an

upper GRS wall supporting the approach slab for the roadway connection. Through this approach, Abu-Hejleh et al. (2000) demonstrated that the use of GRS bridge abutments can also reduce differential settlement between the bridge abutment and the approach slab.

A major GRS bridge abutment project was completed by the Colorado Department of Transportation (CDOT) in 1999 for the Founders/Meadows Bridge in Castle Rock, CO. In this project, GRS walls were built to support the bridge superstructure and the approach roadway. Field measurements during construction indicated the maximum lateral displacement of the lower front facing wall and the maximum settlement of the bridge seat induced by the bridge load were 10 mm and 13 mm, respectively. Measurements also indicated good performance for this GRS bridge abutment during service (Abu-Hejleh et al. 2002). In addition, Lee and Wu (2004) reported good performance of in-service GRS abutments and relatively large loading-bearing capacity from large-scale loading tests. Barrett et al. (2013) also presented successful private sector case studies of GRS abutments over the past 20 years.

Extensive numerical studies have been carried out to investigate the effects of various factors on the deformation responses of GRS abutments for static conditions (Helwany et al. 2003, 2007; Wu et al. 2006; Zheng and Fox 2016), and indicate that reinforcement spacing, backfill soil properties, and bridge load have the most important effects. Zheng and Fox (2016) also found that the horizontal restraint from the bridge superstructure has a significant impact on the abutment deflections. However, these analyses assumed plane strain conditions and 3D effects were neglected. Bergado et al. (2008) investigated 3D effects on the deformation responses of two full-scale embankments and found that 3D analyses were required to accurately consider the effects of the stress state and the geometric layout. Although 2D design methods have been shown to work well for defining the longitudinal reinforcement layout for GRS bridge abutments (Abu-Hejleh et al. 2000, 2002; Lee and Wu 2004; Barrett et al. 2013), 3D effects may play an important role in the design of the side walls and the transverse reinforcement layout.

The objective of this study is to understand the deformation behavior of a hypothetical GRS bridge abutment considering both 3D boundary effects and staged construction effects. Three cases with different reinforcement layouts were studied, and the results from the simulations were synthesized to provide insights into the lower wall lateral facing displacements in both the longitudinal and transverse directions, as well as bridge seat settlements at the centerline of the bridge seat and the edge of the bridge seat.

NUMERICAL MODEL

The finite difference computer program FLAC 3D version 5.0 (Itasca 2012) was used to simulate the deformation response of GRS bridge abutments under static, self-weight loading conditions. Geogrid structural elements were used to model reinforcements and interface elements were used to model interactions between different components, including soil-concrete interface and concrete-concrete interface. Interface elements were characterized using Coulomb sliding model, and the capability of FLAC 3D to handle these types of interfacef makes it well-suited for this study.

Model Configuration

The configuration for the GRS bridge abutment model along with marked components and the finite difference mesh is shown in Figure 1, while the interfaces in the system along the centerline section are shown in Figure 2. The bridge evaluated in this study has a span L = 45 m, width W = 20 m, bridge deck thickness of 2.25 m, bridge seat thickness of 0.4 m, bridge contact length of 2.25 m, lower GRS wall height H = 5 m, upper GRS wall height of 2.65 m (2.25 m + 0.4 m), total abutment height 7.65 m (5 m + 2.65 m), foundation soil depth of 10 m (2H), distance of lower wall facing to lateral boundaries of 20 m (4H), and 100 mm wide expansion joint between the bridge deck and bridge seat on each side. The GRS wall facing consists of modular block concrete elements that measure 0.5 m (length) × 0.25 m (width) × 0.2 m (height). The bridge abutment consists of a bridge seat that measures 21 m (width) × 2.75 m (length) × 2.65 m (height), and sits on top of a reinforced soil mass measuring 19.75 m and 24.5 m in the longitudinal and transverse directions respectively, and offset 0.2 m from the back of the lower front wall facing in the longitudinal direction and 1.75 m from the back of the lower side wall facing in the transverse direction. Each reinforcement layer includes one geogrid placed longitudinally and two geogrids placed transversely, separated by a 25 mm-thick soil layer. Geogrid reinforcements for the lower and upper wall having the same length 3.5 m (0.7H) and the same vertical spacing 0.2 m are rigidly connected to the facing blocks with the upper reinforcements rigidly connected to the back of the bridge seat in the longitudinal direction. With an equivalent unit weight of 5.88 kN/m^3 for the hollow bridge structure, the bridge load on each bridge seat of 298 kN/m [(5.88 kN/m^3 × 45 m × 2.25 m)/2], and the corresponding average applied vertical stress on the bridge seat is 132 kPa [(298 kN/m × 20 m)/(2.25 m × 20 m)]. Since the bottom surface area of the bridge seat (2.75 m × 21 m) is greater than the bridge contact area (2.25 m × 20 m), the average vertical stress on backfill soil is 103 kPa [(298 kN/m × 20 m)/(2.75 m × 21 m)]. The lateral boundaries for the model in the x and y directions were located at a distance of 20 m (4H) and 10 m (2H) away from the lower wall facing blocks to minimize any boundary effects. These boundaries were fixed in the horizontal direction and are free to move in the vertical direction, whereas the bottom boundary was fixed in both horizontal and vertical directions.

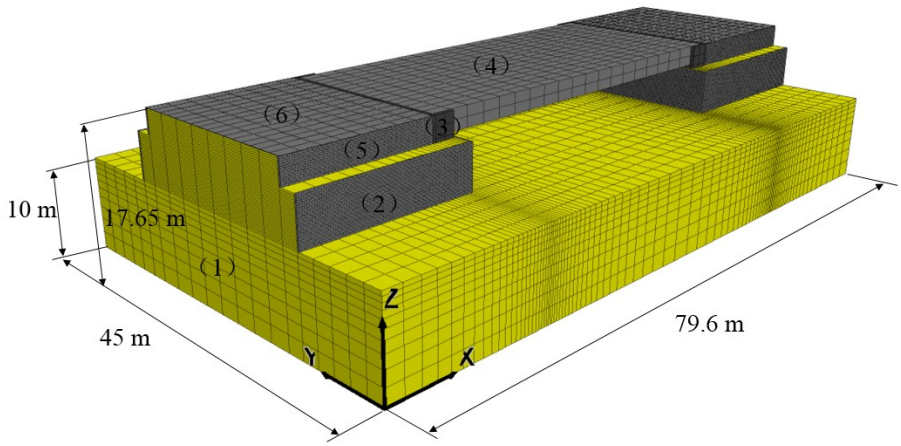

Figure 1. Model configuration and finite difference mesh for the GRS bridge abutment (1: foundation soil, 2: lower GRS wall, 3: bridge seat, 4: bridge deck, 5: upper GRS wall, 6: pavement).

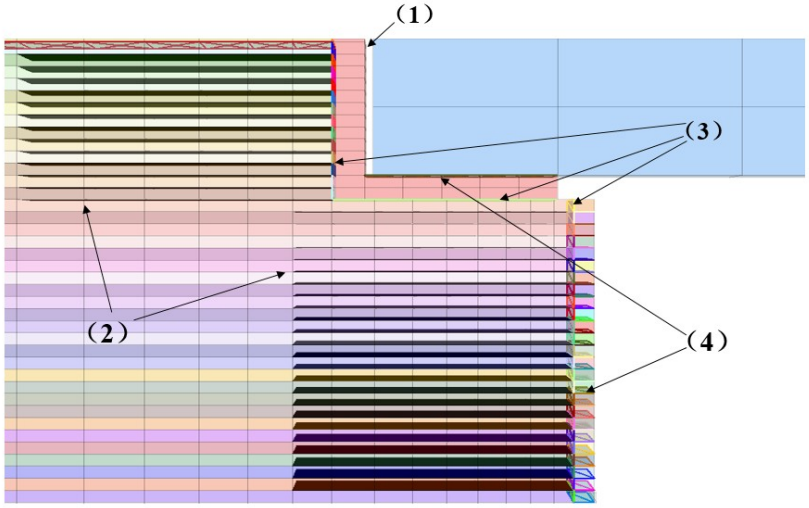

Figure 2. A detailed view in the longitudinal direction of the GRS bridge abutment model (1: expansion joint, 2: geogrid with soil-geogrid interface, 3: soil-concrete interface, 4: concrete-concrete interface).

Material Models and Properties

The concrete facing blocks, bridge seat, bridge deck and approach slabs were modeled as linearly elastic materials having Young's modulus E = 20 GPa and Poisson's ratio v = 0.2. The interface between the blocks has a friction angle of ϕ_{bb} = 36° and apparent cohesion of c_{bb} = 58 kPa, and the normal and shear stiffness are 1000 MPa/m and 40 MPa/m, respectively, as reported by Yu et al. (2016). The apparent cohesion is used to represent the shear keys between the blocks.

Various constitutive models have been developed to describe different aspects of soil behaviors in the past years, among which the Mohr-Coulomb model is a simple and widely used option used in the analysis of slope stability and retaining walls because it only requires two strength parameters to describe the plastic behavior of soils beyond the elastic parameters. As such, the backfill soil was modeled as a linearly-elastic, perfectly-plastic dilatant material with a Mohr-Coulomb failure criterion and non-associated flow rule with a Young's modulus E = 50 MPa, a Poisson's ratio v = 0.3, and an apparent cohesion c = 1 kPa to prevent premature soil yielding in low confining pressure condition and account for additional apparent cohesion due to moisture in the backfill (Hatami and Bathurst 2005). Since the GRS abutment is expected to be far from reaching failure under service loading conditions, a peak friction angle of ϕ = 42° was chosen as a representative value in the simulation. The dilation angle was estimated as follows (Bolton 1986):

$$\phi_p = \phi_{cv} + 0.8\psi \quad (1)$$

where ϕ_p, ϕ_{cv} are the backfill peak and constant volume friction angles, respectively, and ψ is the dilation angle. A value of ϕ_{cv} = 33° was assumed for sand, following typical values reported by Bolton (1986), which corresponds to a dilation angle of ψ = 11.25°. A typical value of unit weight for the backfill soil γ = 19.6 kN/m^3 was chosen for this study. For simplicity, the foundation soil was modeled as the same material as the backfill.

Following the assumption of Yu et al. (2016), the soil-concrete interface friction angle is assumed to be 2/3 of the peak friction angle of the backfill soil, which corresponds to a soil-concrete interface friction angle ϕ_{sb} = 32° [$\tan^{-1}(2/3 \times \tan 42°)$]. The normal and shear stiffness for the soil-concrete interfaces are 100 MPa/m and 1 MPa/m respectively. Considering the embedment of the toe of the GRS wall in the field, a relatively strong toe interface having the same properties as the concrete-concrete interface was selected. The geogrids were simulated using structural elements having isotropic properties and a tensile stiffness of J = 1000 kN/m. The strength reduction factor (R = 2/3) applied to the soil-geogrid interface was the same as that applied for the soil-concrete interface (Yu et al. 2016) resulting in a soil-geogrid interface friction angle of ϕ_{sg} = 32°, with elastic-perfectly plastic sliding permitted. The parameters in the model are summarized in Table 1.

Table 1. Parameter values for constitutive models in the simulations.

Backfill soil	
Unit weight, γ (kN/m^3)	19.6
Young's modulus, E (MPa)	50
Poisson's ratio, v	0.3
Friction angle, ϕ (degrees)	42
Dilation angle, ψ (degrees)	11.3
Apparent cohesion, c (kPa)	1
Concrete	
Unit weight, γ (kN/m^3)	23.5
Young's modulus, E (GPa)	20
Poisson's ratio, v	0.2
Geogrid	
Tensile stiffness, J (kN/m)	1000
Interface properties	
Concrete-concrete interface	
Shear stiffness, $k_{s,bb}$ (MPa/m)	40
Normal stiffness, $k_{n,bb}$ (MPa/m)	1000
Friction angle, ϕ_{bb} (degrees)	36
Apparent cohesion, c_{bb} (kPa)	58
Soil-concrete interface	
Shear stiffness, $k_{s,sb}$ (MPa/m)	1
Normal stiffness, $k_{n,sb}$ (MPa/m)	100
Friction angle, ϕ_{sb} (degrees)	32
Apparent cohesion, c_{sb} (kPa)	0
Soil-geogrid interface	
Shear stiffness, $k_{s,sg}$ (MPa/m)	1
Friction angle, ϕ_{sg} (degrees)	32
Apparent cohesion, c_{sg} (kPa)	0

Modeling Procedures

The construction sequence of the GRS bridge abutment was simulated by first placing the foundation soil, then applying the initial stress state, then solving the system to reach equilibrium under the self-weight of the materials using the small-strain mode in FLAC3D. The large-strain mode was then turned on for the next construction stage to ensure sufficient accuracy for possible large deformations. The lower GRS wall, including 25 soil lifts, reinforcements, and concrete facing blocks was placed and simulated in the correct order (Stage 1). The thickness of each lift was equal to the height of the concrete facing block of 0.2 m. To account for the compaction effort with a roller compactor during construction, a uniform vertical pressure of 8 kPa was applied to the entire surface of each soil layer then removed (Hatami and Bathurst 2005). After adding the interfaces between the facing blocks and between the facing block and backfill soil, the system was then solved to reach equilibrium under the self-weight of the backfill as well as the compaction stresses imposed on the backfill surface. Once the system reached equilibrium, the compaction stress was removed. The same procedure was followed for the remaining lifts until the completion of the lower GRS wall. Then the bridge seat was placed on the reinforced soil masses on either side of the bridge deck (Stage 2) and the bridge deck was placed on the seat (Stage 3). The GRS system was solved to equilibrium at each stage before the next construction sequence. Then, the 13 lifts of backfill in the upper GRS wall were placed, followed by the 50 mm-thick approach roadway, following the same approach used for the lower GRS wall. Finally, the whole GRS bridge abutment system was permitted to stabilize under the final equilibrium state (Stage 4). Since loading in the static construction simulation is symmetric, half of the model was simulated to reduce computational efforts.

SIMULATION RESULTS

Three cases with different reinforcement vertical spacing and lengths were investigated: (a) Case 1: reinforcement vertical spacing S = 0.2 m, length L = 3.5 m (0.7H); (b) Case 2: reinforcement vertical spacing S = 0.4 m, length L = 3.5 m (0.7H); and (c) Case 3: reinforcement vertical spacing S = 0.2 m, length L = 5.0 m (1.0H). The simulation results of primary concern in this study include the lateral displacements for the centerline and the 1/4 off-centerline sections of the lower GRS wall in the longitudinal direction, lateral displacements of the centerline section and the section under the bridge seat (located at a distance 3.2 m from the front facing) of the lower GRS wall in the transverse direction, and the settlements in the centerline as well as the edge of the bridge seat. The lateral displacements of the lower GRS wall in the longitudinal and transverse directions for Case 1 are used as baseline for Cases 2 and 3 to evaluate the deformation behavior of the lower wall in the longitudinal and transverse directions after completion of staged construction.

Lateral Displacement in the Longitudinal Direction in Case 1

The outward lateral displacements for the centerline section of the lower GRS wall after each construction stage described above in Case 1 are shown in Figure 3. The maximum

displacements after completion of the abutment and placement of the deck are 8.4 mm and 26.2 mm, respectively, and these maximum values occur at elevations of z = 2.4 m and 3.6 m, respectively. This indicates the bridge load induces more stress near the top of the lower wall and increases the elevation of the lateral thrust on the GRS wall.

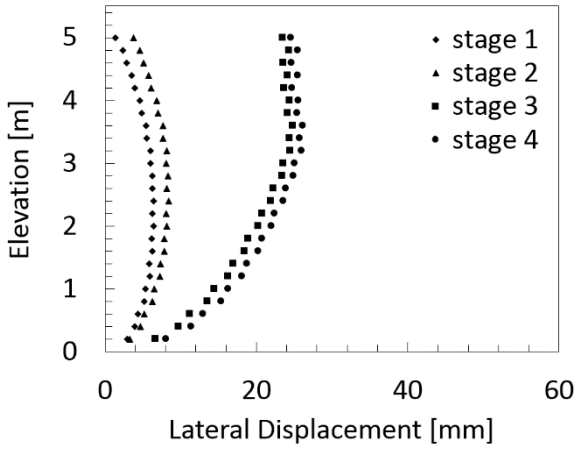

Figure 3. Lateral displacement for the centerline section of the lower GRS wall in the longitudinal direction.

Lateral Displacement in the Transverse Direction in Case 1

The outward lateral displacements for different sections of the lower GRS side wall after each construction stage in Case 1 are shown in Figure 4.

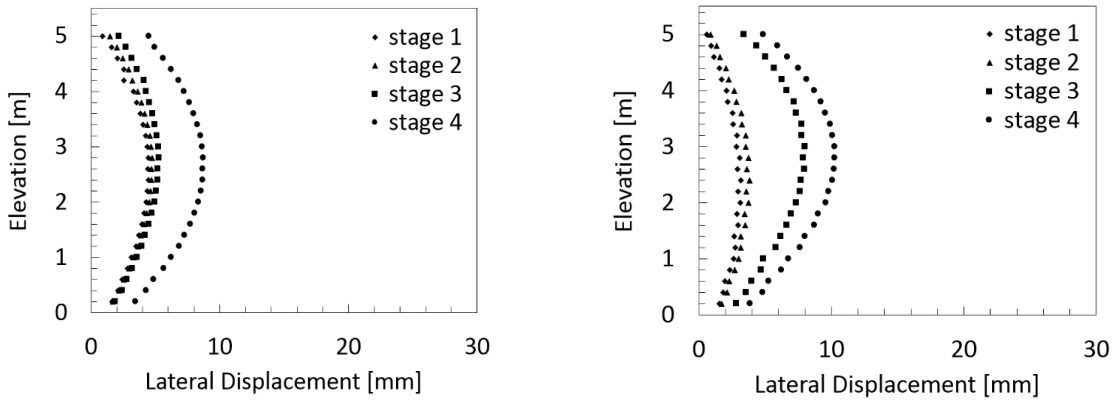

(a) (b)

Figure 4. Lateral displacements of the lower GRS wall in the transverse direction: (a) centerline section of the side wall; (b) section under the bridge seat of the side wall.

Placement of the bridge seat (Stage 2) does not induce much lateral displacements of the lower side wall in both the centerline section and the section under the bridge seat, as observed in Figures 4(a) and 4(b). The maximum displacements for these two sections are 4.8 and 3.8 mm, respectively, at an approximate elevation 3.2 m. Placement of the deck (Stage 3) does not induce much deformation in the centerline section of the side wall (Figure 4(a)), but

leads to 4.2 mm more in the section under the bridge seat (Figure 4(b)). Construction of the upper GRS wall and the approaching pavement (Stage 4) leads to a remarkable increase of 3.6 mm in the centerline section (Figure 4(a)), but a smaller value of 2.2 mm in the section under the bridge seat (Figure 4(b)). Importantly, from Figure 3 and Figure 4(a), it can be concluded that placement of the deck (Stage 3) will have a crucial impact on the deformation behavior of the GRS wall in the longitudinal direction but not on the side wall in the transverse direction; However, construction of the upper GRS wall and pavement (Stage 4) will influence the side walls but not the wall in the longitudinal direction.

Comparisons of the Lateral Displacements in Different Cases

The lateral displacements of the lower GRS wall after completion of staged construction for different cases are shown in Figure 5 for the longitudinal and transverse directions. The centerline section and the 1/4 off-center section of the lower front wall are selected for comparison in the longitudinal direction to study the impact of the stress state effect and any boundary effect, while the centerline section and the section under the bridge seat are selected for comparison in the transverse direction.

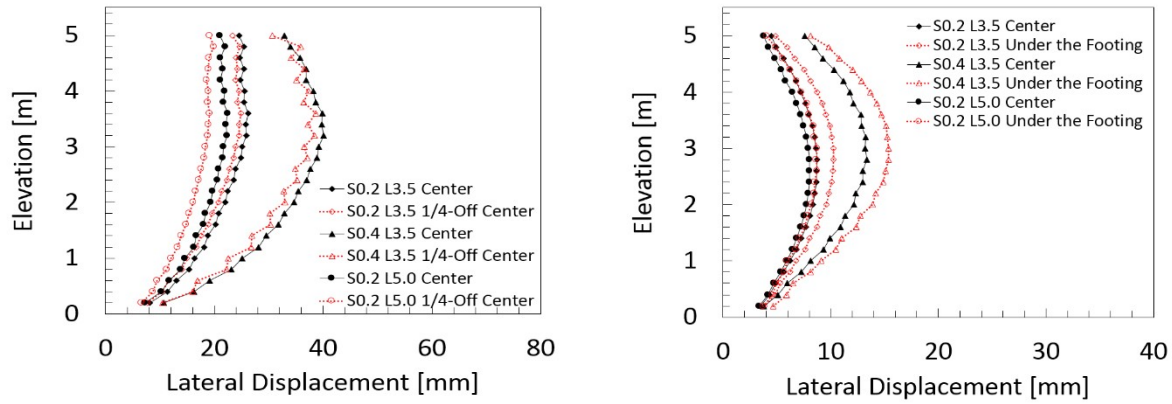

(a) (b)

Figure 5. Comparisons of the lateral displacement of the lower GRS wall after completion of staged constructions: (a) longitudinal direction; (b) transverse direction.

As indicated, reinforcement spacing and length play a significant role on the deformation behavior of the lower GRS wall. The largest lateral deformations occur in Case 2 ($S = 0.4$ m, $L = 3.5$ m) with 40.1 mm and 13.7 mm for the centerline section in the longitudinal and transverse directions respectively, while smallest lateral deformations happen in Case 3 (S = 0.2 m, L = 5.0 m) with the corresponding values 22.4 mm and 8.2 mm. In addition, lateral displacements for the centerline section are relatively larger than the lateral displacements of the 1/4 off-center section in the longitudinal direction and lateral displacements for the section under the bridge seat are relatively larger than the lateral displacements of the centerline section in the transverse direction respectively in all cases, as observed in Figure 5(a) and 5(b), but the differences vary for each of the cases. This is likely due to a combination of the stress state and the global stiffness contributed by the backfill soil and the reinforcement layers.

Bridge Seat Settlements

Settlements of the bridge seat at the centerline as well as at the edge of the bridge seat during construction in each case are plotted in Figure 6. Before placement of the bridge deck (Stage 3), the settlement of the bridge seat is approximately 4.4 mm for all of the cases due to the combined effects of self-weight of the abutment structure, backfill soil and the bridge seat. Settlement increases significantly due to the placement of the bridge deck with the largest increment of 40 mm observed in Case 2 (reinforcement vertical spacing S = 0.4 m, length L = 3.5 m) due to the larger reinforcement vertical spacing. The smallest increment of 25 mm was observed in Case 3 (reinforcement vertical spacing S = 0.2 m, length L = 5.0 m). The settlement at the edge of the bridge seat is approximately the same as the value in the centerline section, which indicates a uniform settlement of the bridge seat and that the bridge seat was relatively rigid.

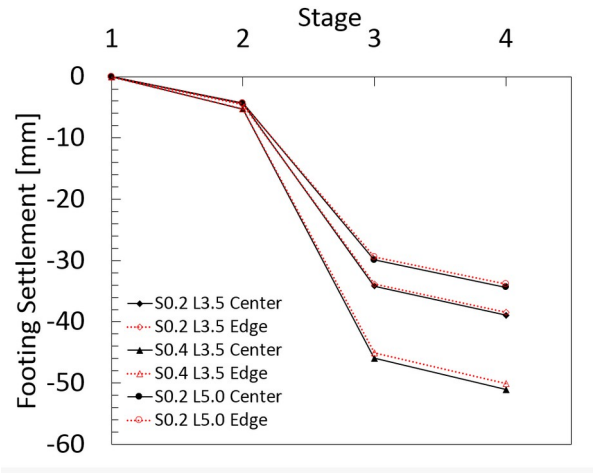

Figure 6. Bridge seat settlements during construction.

CONCLUSIONS

3D deformation behavior of a GRS bridge abutment during staged construction was simulated using the finite difference program FLAC 3D. Placement of the bridge deck led to remarkable lateral displacements of the lower wall in the longitudinal direction and the sections approaching the front facing of the side wall in the transverse direction, as well as settlement of the bridge seat, while construction of the upper GRS wall and pavement will exert a significant impact on the response of the side wall with ignorable effect on the lower GRS wall in the longitudinal direction. Placement of the bridge deck was also found to induce the greatest stresses near the top of the lower front wall and the lower side wall approaching the front facing, indicating that special attention should be paid to these areas during design and construction. In addition, besides the 3D boundary effect and the stress state effect, the reinforcement spacing and length were found to contribute to the global stiffness of the abutment structure and consequently influence the deformation of the GRS bridge abutment both longitudinally and transversely.

ACKNOWLEDGEMENTS

Financial support was provided by the California Department of Transportation (Caltrans) and is gratefully acknowledged. We also thank Dr. Charles S. Sikorsky of the Caltrans Office of Earthquake Engineering for his support and assistance with the project.

REFERENCES

Abu-Hejleh, N., Wang, T., and Zornberg, J.G. (2000). "Performance of geosynthetic-reinforced walls supporting bridge and approaching roadway structures." *Proceedings of Geo-Denver 2000*, 218-243.

Abu-Hejleh, N., Zornberg, J.G., Wang, T., and Watcharamonthein, J. (2002). "Monitored displacements of unique geosynthetic-reinforced soil bridge abutments." *Geosynthetics International*, 9 (1), 71-95.

Bergado, D.T., and Teerawattanasuk, C. (2008). "2D and 3D numerical simulations of reinforced embankments on soft ground." *Geotextiles and Geomembranes,* 26(1), 39-55.

Barrett, R.K., Ruckman, A.C., and Barrett, C.E. (2013). "Geosynthetic-reinforced soil – integrated bridge systems: successful private sector case studies over the last 20 years." *Geosynthetics 2013*, 578-587.

Bolton, M.D. (1986). "The strength and dilatancy of sands." *Géotechnique.* 36(1), 65–78.

Hatami, K., and Bathurst, R.J. (2005). "Development and verification of a numerical model for the analysis of geosynthetic-reinforced soil segmental walls under working stress conditions." *Canadian Geotechnical Journal,* 42(4), 1066-1085.

Helwany, S.M., Wu, J.T., and Froessl, B. (2003). "GRS bridge abutments—an effective means to alleviate bridge approach settlement." *Geotextiles and Geomembranes,* 21(3), 177-196.

Helwany, S.M., Wu, J.T.H., and Kitsabunnarat, A. (2007). "Simulating the behavior of GRS bridge abutments." *Journal of Geotechnical and Geoenvironmental Engineering*, 133(10), 1229-1240.

Itasca Consulting Group, Inc. (2012). Fast Lagrangian Analysis of Continua in 3 Dimensions - 3D Version 5.0. Itasca Consulting Group, Inc., Minneapolis.

Lee, K., and Wu, J.T.H. (2004). "A synthesis of case histories on GRS bridge-supporting structures with flexible facing." *Geotextiles and Geomembranes*, 22, 181-204.

Wu, J.T.H., Lee, K.Z.Z., and Pham, T. (2006). "Allowable bearing pressures of bridge sills on GRS abutments with flexible facing." *Journal of Geotechnical and Geoenvironmental Engineering*, 132(7), 830-841.

Yu, Y., Bathurst, R.J., and Allen, T.M. (2016). "Numerical modeling of the SR-18 geogrid reinforced modular block retaining walls." *Journal of Geotechnical and Geoenvironmental Engineering*, 142(5), 04016003.

Zheng, Y., and Fox, P.J. (2016). "Numerical investigation of geosynthetic-reinforced soil bridge abutments under static loading." *Journal of Geotechnical and Geoenvironmental Engineering*, 142(5), 04016004.